SINTEF
PROCEEDINGS
1

Selected papers from 10th International Conference on Computational Fluid Dynamics in the Oil & Gas, Metallurgical and Process Industries

Progress in Applied CFD

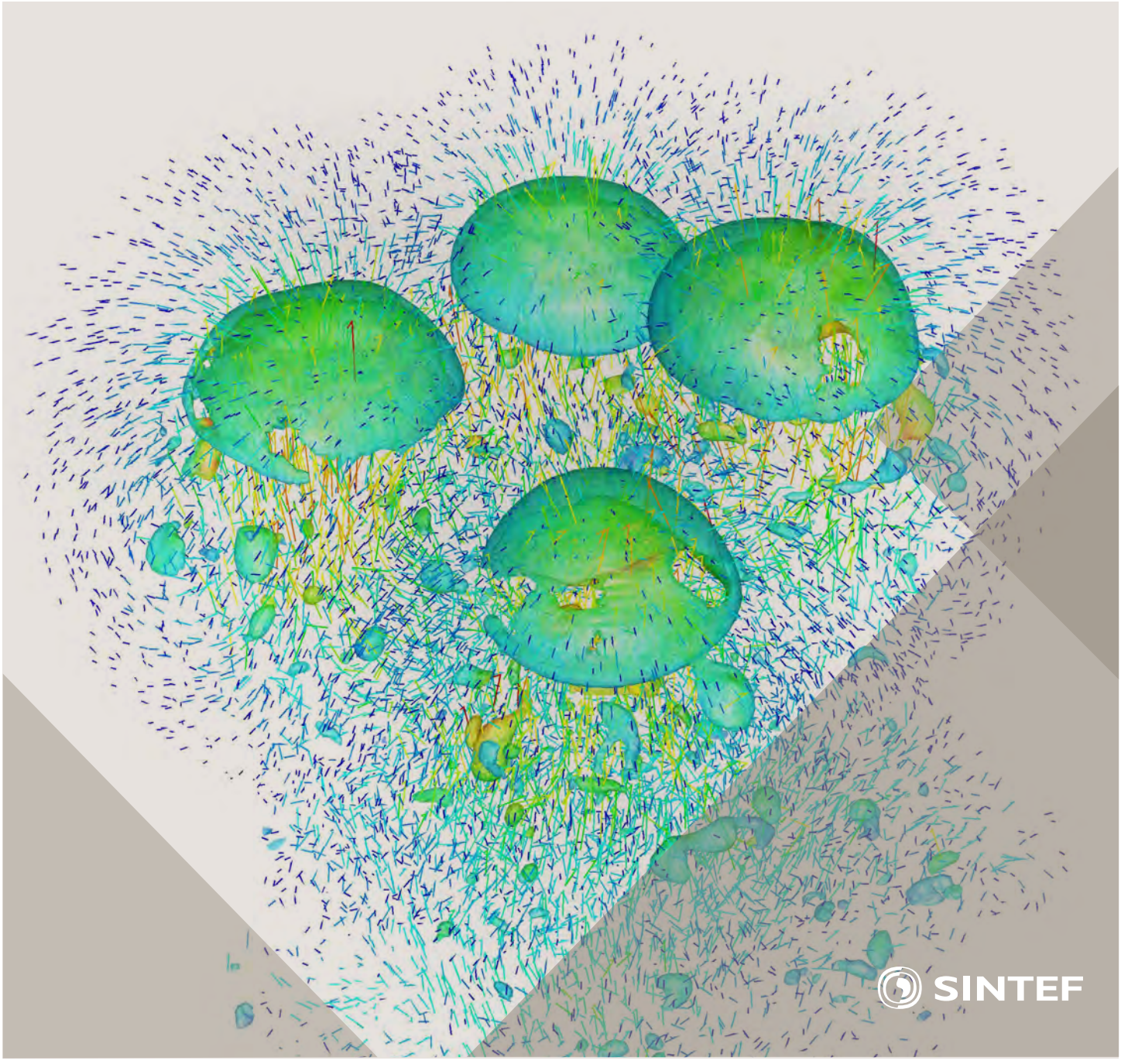

SINTEF Proceedings

Editors:
Jan Erik Olsen and Stein Tore Johansen

Progress in Applied CFD

Selected papers from 10th International Conference on Computational Fluid Dynamics in the Oil & Gas, Metallurgical and Process Industries

SINTEF Academic Press

SINTEF Proceedings no 1
Editors: Jan Erik Olsen and Stein Tore Johansen
Progress in Applied CFD
Selected papers from 10th International Conference on Computational Fluid Dynamics in the Oil & Gas, Metallurgical and Process Industries

Key words:
CFD, Flow, Modelling

Cover, illustration: Rising bubbles by Schalk Cloete

ISSN 2387-4287 (printed)
ISSN 2387-4295 (online)
ISBN 978-82-536-1432-8 (printed)
ISBN 978-82-536-1433-5 (pdf)

60 copies printed by AIT AS e-dit
Content: 100 g munken polar
Cover: 240 g trucard

SINTEF Academic Press
Address: Forskningsveien 3 B
PO Box 124 Blindern
N-0314 OSLO
Tel: +47 22 96 55 55
Fax: +47 22 96 55 08

www.sintef.no/byggforsk
www.sintefbok.no

SINTEF Proceedings
SINTEF Proceedings is a serial publication for peer-reviewed conference proceedings on a variety of scientific topics.
The processes of peer-reviewing of papers published in SINTEF Proceedings are administered by the conference organizers and proceedings editors. Detailed procedures will vary according to custom and practice in each scientific community.

PREFACE

This book contains selected papers from the 10th International Conference on Computational Fluid Dynamics in the Oil & Gas, Metallurgical and Process Industries. The conference was hosted by SINTEF in Trondheim in June 2014 and is also known as CFD2014 for short. The conference series was initiated by CSIRO and Phil Schwarz in 1997. So far the conference has been alternating between CSIRO in Melbourne and SINTEF in Trondheim. The conferences focus on the application of CFD in the oil and gas industries, metal production, mineral processing, power generation, chemicals and other process industries. The papers in the conference proceedings and this book demonstrate the current progress in applied CFD.

The conference papers undergo a review process involving two experts. Only papers accepted by the reviewers are presented in the conference proceedings. More than 100 papers were presented at the conference. Of these papers, 27 were chosen for this book and reviewed once more before being approved. These are well received papers fitting the scope of the book which has a slightly more focused scope than the conference. As many other good papers were presented at the conference, the interested reader is also encouraged to study the proceedings of the conference.

The organizing committee would like to thank everyone who has helped with paper review, those who promoted the conference and all authors who have submitted scientific contributions. We are also grateful for the support from the conference sponsors: FACE (the multiphase flow assurance centre), Total, ANSYS, CD-Adapco, Ascomp, Statoil and Elkem.

Stein Tore Johansen & Jan Erik Olsen

Organizing committee:

Conference chairman: Prof. Stein Tore Johansen
Conference coordinator: Dr. Jan Erik Olsen
Dr. Kristian Etienne Einarsrud
Dr. Shahriar Amini
Dr. Ernst Meese
Dr. Paal Skjetne
Dr. Martin Larsson
Dr. Peter Witt, CSIRO

Scientific committee:

J.A.M.Kuipers, TU Eindhoven
Olivier Simonin, IMFT/INP Toulouse
Akio Tomiyama, Kobe University
Sanjoy Banerjee, City College of New York
Phil Schwarz, CSIRO
Harald Laux, Osram
Josip Zoric, SINTEF
Jos Derksen, University of Aberdeen
Dieter Bothe, TU Darmstadt
Dmitry Eskin, Schlumberger
Djamel Lakehal, ASCOMP
Pär Jonsson, KTH
Ruben Shulkes, Statoil
Chris Thompson, Cranfield University
Jinghai Li, Chinese Academy of Science
Stefan Pirker, Johannes Kepler Univ.
Bernhard Müller, NTNU
Stein Tore Johansen, SINTEF
Markus Braun, ANSYS

CONTENTS

CFD MODELING OF OIL-WATER SEPARATION EFFICIENCY IN THREE-PHASE SEPARATORS

Lanre OSHINOWO*, Ehab ELSAADAWY and Regis VILAGINES
Saudi Aramco Research and Development Center, Dhahran, SAUDI ARABIA
* E-mail: oshinoom@aramco.com

ABSTRACT

Variations in oil properties or water content influence the rate of crude oil-water separation. This presents a challenge for separator operations when conditions change as fields mature, and for the design of new internals to improve separation efficiency. Computational fluid dynamics (CFD) is being used to predict separator vessel hydrodynamics and previous studies of three-phase separators have characterized the dispersed phase with a single droplet size and constant phase properties. Modelling the evolving droplet size during separation is a critical requirement to developing a realistic separator model. Emulsion rheology is also an important phenomena typically overlooked in modeling oil-water separation. In this study, a transient Eulerian multiphase approach coupled with the population balance is used to predict the gas, oil and water separation behavior in three-phase horizontal gas-oil-water gravity separators. Here, the secondary water phase is divided into multiple velocity groups and a number of bins describe the droplet distribution within each velocity group. By considering the dispersed phase fraction in the water-in-oil emulsion rheology and incorporating this into the interphase interaction, a high viscosity emulsion is formed at the interface between the oil and water phases, known as the dense packed layer or zone (DPZ). The resulting DPZ is known to have an effect on oil-water separation efficiency. Experimental data was obtained from a high-pressure pilot scale three-phase separator rig and includes phase flow rates into and out of the vessel and vertical water fraction profiles at two locations in the separator. The data was compared to the CFD predictions of separation efficiency, phase distribution and DPZ thickness in the separator.

Keywords: Emulsion, gravity separation, three-phase, separator, oil, multiphase, population balance, CFD.

NOMENCLATURE

a Coalescence rate, [m^3/s].
c_1, c_2, c_3 Coalescence rate empirical constants, [-].
B Interfacial force constant, [N.m^2].
B Birth rate, [1/s].
C_D Droplet drag coefficient, [-].
d Droplet diameter, [m].
D Death rate, [1/s].
f Drag function, [-].
f Friction factor, [-].
f_i Discrete bin fractions, [-].
$\vec{g}$ Gravitational acceleration, [m/s^2].
g Breakage frequency, [1/s].
h Collision frequency of droplets of volume V and V', [1/s].
$h_{w,l}$ Interface and liquid level, [m].
$\bar{\bar{I}}$ Unit tensor, [-].
k_B Boltzmann constant, [J/K].
K Loss coefficient, [-].
K_{ij} Mean interphase momentum exchange, [kg/m^3.s].
m Mass transfer rate, [kg/s].
M Number of bins per phase/velocity group, [-].
N Number of velocity groups, [-].
p Pressure, [Pa].
Pe Peclet number, [-].
Q Volumetric flow rate, [m^3/s].
Re Reynolds number, [-].
S population balance equation source term, [1/m^3].
T Temperature, [K].
u, v, w Components of velocity, [m/s].
V Droplet volume, [m^3].
x, y, z Coordinates, [m].

Greek Symbols
α Phase fraction, [-].
$\beta(V|V')$ probability density function of droplets breaking from volume V' to V, [-].
λ Coalescence efficiency of a binary droplet pair, [-].
μ Viscosity, [kg/m.s].
ρ Mass density, [kg/m^3].
σ Interfacial tension, [N/m].
τ Particle relaxation time, [s].

Sub/superscripts
g, w, o Gas, Water, Oil.
c Continuous phase.
d Dispersed phase.
l Liquid.
m Mixture.
i, j, k Indices i, j, k.

INTRODUCTION

The separation of gas, oil and water by gravity is found throughout oil and gas production operations. The multiphase separator is the first unit in the production line between the production manifold and the pipeline transport. In offshore production, the multiphase flow is separated into the requisite streams top-sides while onshore, the Gas-Oil Separation Plants (GOSP) handle the separation. Horizontal gravity separators are high-aspect ratio cylindrical vessels with a relatively short entrance region for disengagement of gas and liquid. To improve the efficiency of separation while reducing the overall vessel dimensions, various types of "internals" – plate, vane or cyclonic momentum breakers at the vessel inlet, coalescing plates, solid and perforated baffle plates, flow

straighteners, foam breakers, weirs, mist eliminators, electrocoalescers – are all used to promote gas-liquid and liquid-liquid separation. Computational fluid dynamics (CFD) has long been recognized as a promising tool in design, sizing and retrofit studies of multiphase separators. In the CFD work by Hansen and co-workers, the three-phase separator was modeled by considering different two-phase regions of the separator: a freeboard region with dispersed liquid droplets in gas, and the liquid bath with water or oil droplets dispersed in oil or water (Hansen *et al*., 1991, Hansen and Rørtveit, 2005). The emulsion viscosity was modeled by changing the continuous phase oil viscosity with the local water volume fraction. Another approach has been to model the oil-water emulsion as a mixture using the volume of fluid model and determine the water separation efficiency by tracking a droplet distribution with an uncoupled Lagrangian dilute-phase particle tracking model (Laleh *et al*., 2012). The presumption of dilute flow may be valid for droplets dispersed in the gas phase but not in the liquid phase. The water phase accumulates and the dilute conditions become dense phase conditions in regions of the separator, making the dilute Lagrangian approach inappropriate for modelling the oil-water phase separation. The Eulerian multiphase modelling approach is the most appropriate to describe complex phase rheology, phase separation and inversion in oil-water emulsions that exist in continuous and batch separators (Hallanger *et al*., 1996). Phases are treated as interpenetrating continua in the Eulerian multiphase approach and phase volume fractions add up to one in each cell of the computational domain. A momentum transport equation is solved for each phase in addition to a continuity equation. Interphase interaction forces, like drag and lift, are modeled using momentum exchange coefficients. Several recent studies applied Eulerian multiphase models but the dispersed water phase was modeled with a constant droplet diameter (Vilagines and Akhras, 2010, Kharoua *et al*., 2012). While these studies and others have shown that CFD helps to elucidate the macroscopic parameters, such as, flow patterns, pressure drop, and phase residence time, CFD has been unable to predict separation performance accurately (Laleh *et al.*, 2012, Frising *et al*, 2006). The main reasons for these shortcomings have been a lack of a comprehensive treatment of the oil-water emulsion rheology and the poly-disperse nature of the multiple phases. It is widely recognized that the dispersed phase size distribution in liquid-liquid dispersions influences the separation kinetics in gravity separation (Henscke *et al*., 2002). The size distribution evolves with transport through the separation vessels due to varying shear, turbulence, and due to the effects of surface active agents naturally present or injected upstream of the GOSPs. In this study, a CFD methodology to model GOSPs is presented. The population balance model is used here to predict the evolving droplet size distribution in the oil emulsion and its viscosity varies with water content. Experimental data were obtained from a pilot-scale high-pressure, three-phase horizontal gravity separator, and compared to the CFD model results.

EXPERIMENTAL

The experimental data obtained for the CFD model study was obtained from a pilot scale, high-pressure, horizontal, three-phase gas-oil-water separator flow loop at the IFP Energies Nouvelles site in Solaize, France (Pagnier *et al.*, 2008). The closed flow loop, as illustrated in Figure 1, consists of feed tank for the oil and water and a gas compression system. The flow loop has instrumentation to quantify the flows in and out of the separator vessel. The mass flow rate, pressure and temperature for each phase are controlled. The temperature control is achieved using separate heat exchangers for cooling and for heating. The oil and water phases are mixed in a Y-branch followed by two static vane mixers, one upstream and the other downstream of the heat exchangers. The gas is introduced after the second liquid static mixer. The three-

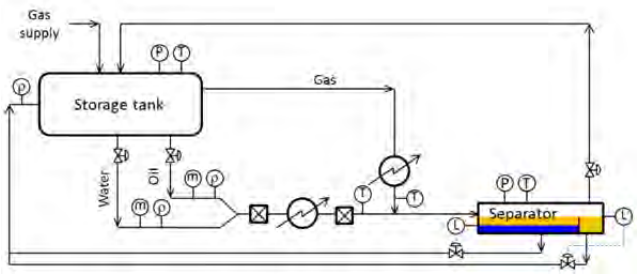

Figure 1. Pilot-scale, high-pressure, horizontal, three-phase gas-oil-water separator flow loop at the IFPEN (Pagnier, et al. 2008)

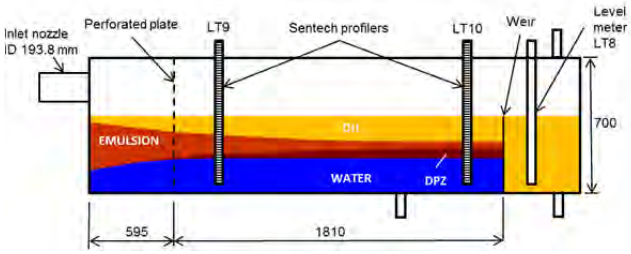

Figure 2: Schematic of the high-pressure, three-phase, pilot separator (ID 700mm, Length 3000mm).

phase flow then travels approximately 15 m through a 3-inch (ID 73.66 mm) line to the multiphase separator vessel. The separator vessel is 700 mm in diameter and 3000 mm in length and is illustrated in Figure 2. The separator inlet is an 8-inch diameter nozzle (ID 193.8 mm) while 2-inch (ID 47.3 mm) nozzles are used for the gas, oil and water outlets. A perforated plate, located 595 mm from the inlet flange, separates the entry region from the settling zone in the vessel that extends 1810 mm to the weir. The perforated plate is 10 mm thick with 13 mm holes arranged in a triangular pattern with a 54% open area. The weir height is 400 mm from the vessel bottom. The evolution of the separating water phase is measured *in-situ* in the separator using two commercially-available electrical capacitance profilers (Schuller *et al.*, 2004). The two profilers, LT9 and LT10 (Figure 2), are mounted vertically just downstream of the perforated plate (750 mm from inlet flange) and upstream of the weir (2250 mm from inlet flange), respectively. The profilers determine the spatial distribution of the water phase and the interface boundaries between the water and emulsion, emulsion and oil, oil and gas. The profilers consist of a linear array of elements with each element having a single capacitance electrode. The elements are typically spaced every 10 mm and give a measurement related to permittivity that is calibrated to the water/brine volume fraction. It is then possible to ascertain the height of the water-emulsion and oil-gas interface from the maximum and minimum permittivity measurements. The dense packed zone (DPZ) forms in the emulsion layer above the water interface. In this zone, the water fraction typically exceeds the inlet water fraction. The height of the DPZ is interpreted from an inflexion in the water fraction profile, measured from the LT10 profiler as illustrated in Figure 3, typically corresponding to water fraction in excess of the inlet value. A water fraction of 0.1 defines the boundary between the emulsion and the oil layers. The oil/liquid level in the vessel is measured by the level transmitter LT8 and controlled by the valve on the oil outlet line. Alternatively, the liquid level is controlled by the weir. The water-emulsion interface level is controlled using the water outlet control valve, based on the interface level measurement from the LT10 profiler. The oil and water discharged from the separator are circulated back to the feed tank where the phases separate and return to the flow loop. The oil-water feed tank volume is 10 m^3 while the separator vessel has a capacity of approximately 1 m^3. The oil used is a Saudi Arabian light crude oil with an API gravity

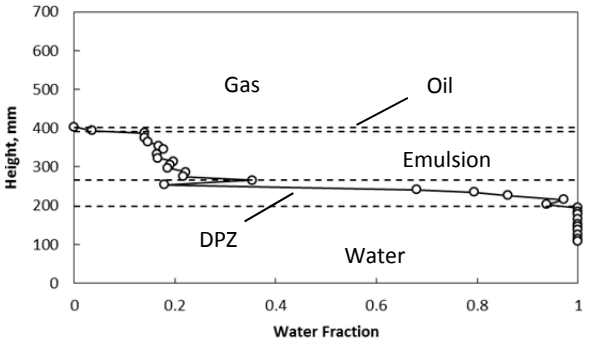

Figure 3. Measured water fraction obtained at the LT10 capacitance probe showing the dense packed emulsion zone.

of 35. The water is a brine mixture with 50 g/L NaCl. A demulsifier is added to the aqueous phase in a dosage of 50 ppm Clariant PT 4688. The gas phase is a mixture consisting of 97.8% methane, 1.1% nitrogen, 0.8% ethane, 0.2% propane, and 0.1% carbon dioxide. The operating temperature and pressure are 45°C and 24 bar, respectively. The experimental conditions selected for this paper are listed in Table 1.

Table 1. Experimental Conditions.

Oil Flowrate Q_o	m^3/h	3.40
Water Flowrate Q_w	m^3/h	1.50
Liquid Flow Q_l	m^3/h	4.9
Gas Flowrate Q_g	Am^3/h	13.95
Gas Fraction $Q_g/(Q_l+Q_g)$	-	0.74
Water Cut Q_w/Q_l	-	0.31
Water Level h_w	mm	199
Liquid Level h_l	mm	405*

** Level controlled by weir.*

MODEL DESCRIPTION

An Eulerian-Eulerian multiphase method was used to model the characteristics of the multiphase dispersion encountered in gravity separators. The liquid-dispersions found in gravity separation can be characterized as dense with the volume fraction ranging from zero to 100%. With the dispersion of gas bubbles and water droplets in the continuous oil phase, the oil phase is considered in this work to be the primary phase while the gas and water phases are considered secondary phases. The poly-dispersity of the secondary-phase water droplet population is modeled with the population balance method.

Multi-fluid Multiphase Model

The conservation equations are derived by ensemble averaging the local instantaneous balance for each phase. The continuity equation for phase *j* is

$$\frac{\partial}{\partial t}\left(\alpha_j\rho_j\right)+\nabla\cdot\left(\alpha_j\rho_j\vec{v}_j\right)=\sum_{i=1}^{n}\left(\dot{m}_{ij}-\dot{m}_{ji}\right) \quad (1)$$

where α_j, ρ_j and $\vec{v}_j$ are the phase volume fraction, density and velocity, and $\dot{m}$ is the mass transferred between phases. The momentum balance for phase *j* is

$$\frac{\partial}{\partial t}\left(\alpha_j\rho_j\vec{v}_j\right)+\nabla\cdot\left(\alpha_j\rho_j\vec{v}_j\vec{v}_j\right)=-\alpha_j\nabla p+\nabla\cdot \alpha_j\mu_j\left[\left(\nabla\vec{v}_j+\nabla\vec{v}_j^{T}\right)-\tfrac{2}{3}\nabla\cdot\vec{v}_j\bar{\bar{I}}\right]+\sum_{i=1}^{n}\left(K_{ij}\left(\vec{v}_i-\vec{v}_j\right)+\dot{m}_{ij}\vec{v}_{ij}-\dot{m}_{ji}\vec{v}_{ji}\right)+\alpha_j\rho_j\vec{g} \quad (2)$$

where p is pressure, μ is viscosity, $\bar{\bar{I}}$ is the unit tensor, and $K_{ij}\left(=K_{ji}\right)$ is the mean interphase momentum exchange coefficient and can be written in general form as:

$$K_{ij}=\frac{\alpha_i\alpha_j\rho_j f}{\tau_i} \quad (3)$$

The terms f and τ_i are the drag function and particle relaxation time, respectively, expressed as

$$f=\frac{C_D Re}{24} \quad (4)$$

and,

$$\tau_i=\frac{\rho_j d_i^2}{18\mu_m} \quad (5)$$

where d_i is the Sauter mean diameter coupling the momentum equations to the population balance equation. For settling or rising droplets, the drag originates from viscous surface shear and the pressure distribution, or form drag, around the droplet. For dilute dispersions, the droplets can settle or rise without interacting with neighbor droplets. For small droplets in the viscous regime, the Stokes law determines the terminal velocity in dilute or unhindered conditions. In the dense dispersions found in oil-water batch and continuous gravity separation, the drag function must include the influence of neighbor droplets and hindered settling. The Schiller-Naumann correlation for drag coefficient C_D is modified for hindered settling in dense suspensions using a mixture or emulsion Reynolds number Re_m based on the emulsion viscosity μ_m described later:

$$C_D=\frac{24}{Re_m}\left(1+0.15Re_m^{0.687}\right) \quad (6)$$

$$Re_m=\frac{\rho_c|u_d-u_c|d_d}{\mu_m} \quad (7)$$

where subscripts *c* and *d* refer to the continuous and dispersed phases, respectively. The drag force is the only contribution to the interphase interaction that was considered. Other forces including virtual mass force, transverse lift force, or wall lubrication force were not considered given droplet Reynolds numbers of the order 0.01 for water-in-oil dispersions relevant to crude oil separation. The turbulent dispersion force – that contributes to diffusion in dispersed flows – was not considered here. The mixture or emulsion viscosity depends on the viscosities of the dispersed and continuous phases, the concentration of the dispersed phase, the shear field, the droplet size distribution, temperature, and the emulsion stability. The interfacial stability is dependent on many non-hydrodynamic factors including the crude oil heavy fraction, solids, temperature, droplet size and distribution, pH, salinity, and composition (Kokal, 2005, Sanfeld and Steinchen, 2008). Brinkman derived the following equation for emulsion viscosity for suspensions of hard spheres (Brinkman, 1952):

$$\mu_m=\mu_c(1-\alpha_d)^{-2.5} \quad (8)$$

Krieger and Dougherty extended Brinkman's correlation by including the contribution of the maximum packing value (Krieger and Dougherty, 1959):

$$\mu_m=\mu_c\left(1-\frac{\alpha_d}{\alpha^*}\right)^{-2.5\alpha^*} \quad (9)$$

where α^* is the packing concentration of 0.64 for hard spheres in non-equilibrium reaching the limit of 0.74 for a hexagonal close packed structure. With increased pressure, droplets can deform and the maximum packing value α^* could approach unity. Ishii and Zuber extended the Krieger-Dougherty correlation by including a viscosity factor in the exponent (Ishii and Zuber, 1979):

$$\mu_m=\mu_c\left(1-\frac{\alpha_d}{\alpha^*}\right)^{-2.5\alpha^*\mu_*} \quad (10)$$

$$\mu_*=\left(\frac{\mu_d+0.4\mu_c}{\mu_d+\mu_c}\right) \quad (11)$$

Mills derived the following equation for the apparent shear viscosity of a concentrated suspension of hard spheres in a Newtonian fluid based on a free cell model (Mills, 1985):

$$\mu_m=\mu_c\frac{1-\alpha_d}{(1-\alpha_d/\alpha^*)^2} \quad (12)$$

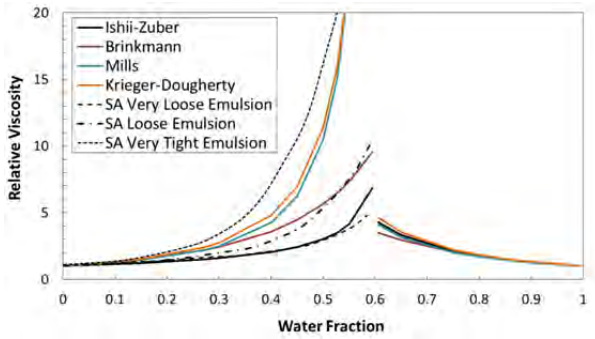

Figure 4. Relative viscosity (μ_m/μ_c) for Arab Light crude (API ~ 35) and brine (50 g/L) at 45°C. (Arabian crude emulsions from Kokal, 2005).

The emulsion viscosity equations are plotted in Figure 4 for a Saudi Arabian Light crude oil emulsion at 45°C with phase inversion at 60% water. In crude oil emulsions, the emulsion viscosity can be of the order 10 to 100 more than the continuous phase viscosity (Marsden and Mad, 1975). For comparison are the emulsion viscosity curves for very loose and very tight Arabian crude emulsions (Kokal, 2005). The terms "loose" and "tight" refer to the relative stability of the emulsion.

Population Balance Model

A population balance equation is coupled with the turbulent multiphase momentum equations conveniently describing the water droplet size distribution (Ramkrishna, 2000). The general population balance equation is written as a continuity statement of the droplet number density function:

$$\frac{\partial}{\partial t}[n(V,t)] + \nabla \cdot [\vec{v} n(V,t)] = S(V,t) \qquad (12)$$

The spatial location of the particle is an "external coordinate" in the particle state vector, while the droplet volume V is an "internal coordinate" of the population distribution. The source term $S(V,t)$ for breakage b and coalescence c due to birth (B) and death (D) rates is further expanded as:

$$S(V,t) = B_b(V,t) - D_b(V,t) + B_c(V,t) - D_c(V,t) \qquad (13)$$

The closure of Equation (12) requires a derivation of the source terms in Equation (13) above.

Breakage and Coalescence Kernels

The breakage rate kernel is the product of the breakage frequency $g(V')$ and the probability density function (PDF) $\beta(V|V')$ of droplets breaking from volume V' to V. The birth rate of droplets of volume V due to breakage is

$$B_b = \int_{\Omega_V} p\, g(V')\, \beta(V|V')\, n(V')\, dV' \qquad (14)$$

where $g(V')\, n(V')\, dV'$ droplets of volume V' break per unit time, producing for p child droplets, $p\, g(V')\, n(V')$ droplets of which a fraction $\beta(V|V')dV$ represents droplets of volume V (Luo and Svendsen, 1996). The breakage PDF $\beta(V|V')$ is also referred to as the daughter size distribution function where the fragments or daughter droplet mass must equal the original droplet mass. The death rate of droplets due to breakage is

$$D_b = g(V)n(V) \qquad (15)$$

There are several different models for determining the breakage frequency and the breakage PDF to compute the breakage rate of the droplets. The coalescence kernel $a(V-V',V')$ is a product of the collision frequency $h(V-V',V')$ between droplets of volume V and V', and the coalescence efficiency $\lambda(V-V',V')$. The coalescence efficiency is the probability that droplets of volume V will coalesce with droplets of volume V'. The birth rate of droplets due to coalescence is

$$B_c = \frac{1}{2}\int_0^V a(V-V',V')\; n(V-V')n(V')\, dV' \qquad (16)$$

The death rate of droplets due to coalescence is

$$D_c = \frac{1}{2}\int_0^V a(V,V')\; n(V)n(V')\, dV' \qquad (17)$$

In the three-phase or two-phase separator settling zone, the complex oil-water emulsion evolves primarily due to droplet coalescence while other phenomena including breakage, dissolution, aggregation, and flocculation occur to a lesser. Droplet breakage is more important at the separator entrance region where the multiphase flow is highly turbulent. Along with droplet breakage and mass transfer, coalescence influences the evolution of the droplet size distribution in liquid-liquid emulsions. Grimes (2012) developed a coalescence rate kernel in the context of batch gravity separation of oil-water emulsions. Droplet pair collisions are considered to depend on both Brownian and gravitational coalescence (Simons *et al.*, 1986). The collision frequency is (Grimes 2012):

$$h(d_k,d_j) = c_1 \frac{k_B T}{6\mu}\frac{(d_k+d_j)^2}{d_k d_j}\left[1 + Pe + 4.496 Pe^{\frac{1}{3}}\right] \qquad (18)$$

Where b_1 is an empirical fitting parameter and Pe is the sphere pair Peclet number,

$$Pe = \frac{\pi}{12}\frac{(\rho_d-\rho_c)\vec{g}}{k_B T}(1-\alpha)^{c_2} d_k d_j \left|d_k^2 - d_j^2\right| \qquad (19)$$

The coalescence efficiency is expressed as the ratio of coalescence time and the contact time:

$$\lambda(d_k,d_j) = \exp\left[-\frac{1.046}{c_3}\frac{\mu(\rho_d-\rho_c)\vec{g}}{\sigma^{3/2}B^{1/2}}\left[\frac{d_k d_j}{2(d_k+d_j)}\right]^{9/2}\right] \qquad (20)$$

The empirical constant b_2 influences the hindered settling contribution to the collision frequency, based on the Richardson-Zaki hindered settling correlation, while b_3 is used to adjust the coalescence time. The coalescence efficiency is also dependent on an interfacial force constant B, which can be related to the surfactant concentration (Grimes, 2012; Kralova *et al.*, 2011). Generally, there are recognized weaknesses with coalescence kernels, including: the derivation of the collision frequency based on the kinetic theory of gases, the lack of history to capture the cumulative effects during the coalescence process, and other empiricism (Liao and Lucas, 2010). The kernels are relatively simplistic given the complexity of the system and the phenomena.

Population Balance Equation Solution Method

To model separation of the dispersed water phase from the oil phase, the solution to the population balance cannot be based on a shared velocity field since droplets of different sizes will rise or settle at different velocities. The droplet size distribution can range over two to three orders of magnitude or more, and the distribution can be mono- or multi-modal. Multivariate methods incorporating several velocity classes are required to model this tight coupling between the droplet size distribution and the secondary phase velocity distribution. There are a number of multivariate methods described in the literature but the Inhomogeneous Discrete Method (IDM) (Frank *et al.*, 2005, Sanyal *et al.*, 2013) will be used in this work. The population balance equation is written for the IDM in terms of volume fraction of particle or droplet size i and solved here for all discrete bin fractions f_i :

$$\frac{\partial}{\partial t}(\rho\alpha f_i) + \nabla\cdot(\rho\alpha f_i v_i) = \rho V_i\left(B_{c,i} - D_{c,i}\right) \qquad (21)$$

where ρ is the density of the secondary phase. The secondary phase is divided into N velocity groups or phases, each with M bins per phase for a total of $N \times M$ bins. The sum of

coalescence mass sources for all phases is zero, while each phase or bin could have a non-zero net mass source. Each bin is advected by phase velocity u_i and $\alpha f_i (= \alpha_i)$ is the volume fraction of bin i, defined for secondary phase 0 to $N-1$ as

$$\alpha_i = N_i V_i \tag{22}$$

$$N_i(t) = \int_{V_i}^{V_{i+1}} n(V,t)dV \tag{23}$$

The droplet coalescence birth and death rates are

$$B_{c,i} = \sum_{k=1}^{N}\sum_{j=1}^{N} \alpha_{kj} N_k N_j x_{kj} \xi_{kj} \tag{24}$$

$$D_{c,i} = \sum_{j=1}^{N} \alpha_{ij} N_i N_j \tag{25}$$

where the coalescence rate $\alpha_{ij} = a(V_i, V_j)$ and

$$\xi_{kj} = \begin{cases} 1 & \text{for } V_i < V_c < V_{i+1}, \text{ where } i \le N-1 \\ 0 & \text{otherwise} \end{cases} \tag{26}$$

V_c is the particle volume resulting from the coalescence of droplets k and j defined as

$$V_c = \left[x_{kj} V_i + (1 - x_{kj}) V_{i+1}\right] \tag{27}$$

and

$$x_{kj} = \frac{V_c - V_{i+1}}{V_i - V_{i+1}} \tag{28}$$

Numerical Setup and Boundary Conditions

Model

A carefully constructed mesh consisting predominantly of hexahedral cells was built on a 180° symmetrical geometry using the cut-cell method (Figure 5). The resulting 1.4 million cell mesh consists of 8 mm cells in the bulk of the vessel and 4 mm cells in the outlet nozzles. Mesh refinement was applied at the walls.

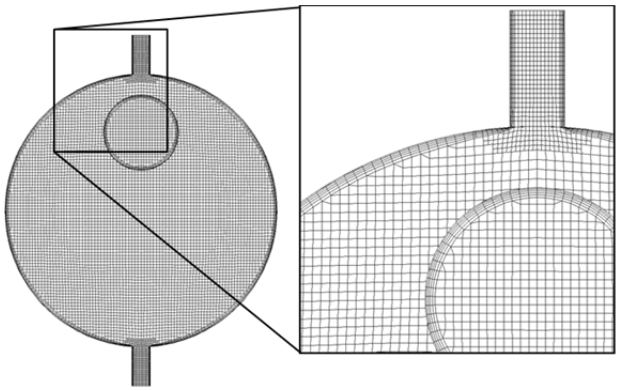

Figure 5. End-view of mesh showing details at the walls and the outlet nozzles.

Initial Droplet Size Distribution

In the pipe approaching the separator inlet, droplet size distribution evolves due to varying shear, and turbulence, the effects of surface-active agents naturally present, and the demulsifier. At the entrance to the separator, the complex oil-water emulsion continues to evolve due to breakage and coalescence. In the settling zone, coalescence processes are dominant and breakage, dissolution, aggregation, and flocculation occur to a lesser extent. In the absence of droplet size measurements at the separator inlet, the initial droplet diameter distribution is determined from the maximum stable droplet size d_{max} (Hinze, 1955)

$$d_{max} = \frac{0.725}{\left(\frac{\rho_l}{\sigma}\right)^{3/5} \epsilon^{2/5}} \tag{29}$$

where the mean turbulent energy dissipation per unit mass ϵ is

$$\epsilon = f \frac{v_m^3}{2D} \tag{30}$$

and the friction factor f is

$$f = F_2 + \frac{(F_1 - F_2)}{\left(1 + \left(Re_m/t\right)^c\right)^d} \tag{31}$$

where $F_1 = a_1 Re_m^{b_1}$ and $F_2 = a_2 Re_m^{b_2}$ (Garcia, *et al.* 2007). The parameters a_1, a_2, b_1, b_2, c, d and t are dependent on the flow regime. The minimum droplet size is determined from (Vielma, *et al.* 2008)

$$d_{min} = 8\frac{\sigma}{g\rho_l v_l^2} \tag{32}$$

The mean droplet diameter is

$$d_{mean} = 0.4 d_{max} \tag{33}$$

Using a 39−bin cumulative volume fraction distribution for water droplets dispersed in an Arabian Light crude oil (API > 35) with added demulsifier, each bin is assigned a droplet size based on a Rosin-Rammler distribution:

$$d_{i_0} = d_{mean}[-ln(1-\alpha_i)]^{1/n} \tag{34}$$

where α_i is the $i-th$ bin fraction and the spread parameter n is 2. Figure 6 shows the cumulative droplet size distribution at the separator inlet.

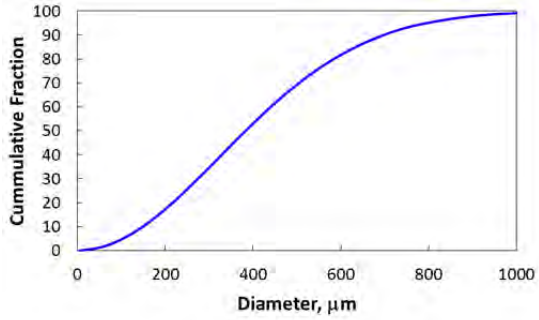

Figure 6. Cumulative droplet size distributions at the separator inlet.

Inlet Velocity Boundary Conditions

The inlet phase distributions are based on the incoming flow regime. For the experimental conditions modeled, the flow regime in the 3" pipe is stratified or intermittent elongated bubble based on three-phase gas-oil-water studies (Keskin *et al.*, 2007). The transition to the 8" nozzle will alter the flow regime to a separated or stratified flow regime. Though still developing through the reduction from the pipe to the nozzle, the larger cross-section will allow the gas to disengage and the flow regime will tend to stratified flow. A uniform velocity condition for each phase is assumed and the distribution of oil and water is considered fully mixed at the velocity inlet boundary. The inlet phase distribution is applied at the boundary using a user-defined function.

Perforated Plate

The perforated plate, described in the experimental section, is modeled as a porous media (cell zone). The inertial resistance of the porous media is based on the product of the loss coefficient K and the local kinematic head and applied as a momentum source in the z-direction for the porous cell zone. The loss coefficient K is not constant but varies with the local Reynolds number as shown in Figure 7. A user-defined function reads and interpolates a table of $\log(K)$ as a function of the $\log(Re)$ to return a value for K at the local Re based on the local approach velocity. A high loss coefficient value of 100,000 is applied in the transverse directions of the perforated plate cell zone.

Outlet Pressure Conditions

If the liquid outlet boundary pressure P_{outlet} is initially set assuming separated phases (A in Figure 8 below), the water interface will drop until a steady-state distribution of water-in-oil (w/o) emulsion is reached (B). Since the w/o concentration distribution is not known *a priori*, the outlet pressure (P_{outlet}) is initially estimated based on

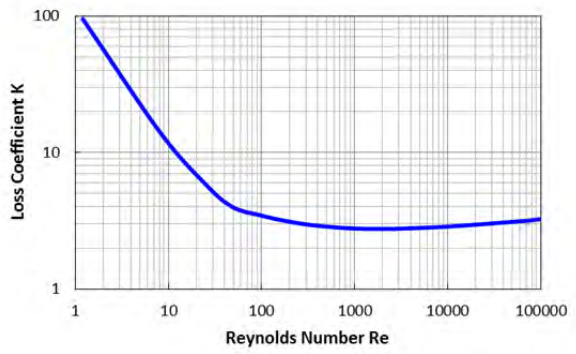

Figure 7. Perforated plate loss coefficient as a function of the perforation Reynolds number.

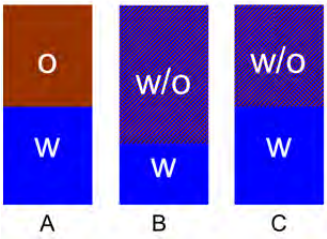

Figure 8. Illustration of the vertical column of oil (O), emulsion (w/o) and water (W) layers in the separator vessel.

$$P_{outlet} = \rho_{w/o} g h'_{w/o} + \rho_w g h_w \qquad (35)$$

and adjusted during the calculations in response to the interface level set point h_w. The interface level is determined from the average height of an iso-surface of water fraction of value 0.9 created at the intersection with an axial plane at the LT9 and LT10 locations. The outlet pressure adjustment is executed manually or automatically. Here, an automatic interface level control is applied using a Proportional-Integral-Derivative (PID) controller algorithm to efficiently manage the simulation over long run-times. The outlet pressure is controlled to the set point of water-emulsion interface height (See Table 1).

Solution

The three-phase system was modeled with the Eulerian multiphase model in ANSYS FLUENT 14.5 (ANSYS Inc., 2012). A transient solution was obtained for each run with a fixed time-step of 0.5 seconds. The primary phase is the oil phase with water and gas as secondary phases. Dispersed gas bubbles have a constant diameter of 2 mm. The Inhomogeneous Discrete Model is used and three secondary phases discretize the water phase with two bins per phase. The droplet diameter range for each phase is determined from the droplet size distribution in Figure 6. An initial value for each of the six bin fractions is specified at the inlet boundary according to the droplet size distribution. The Grimes coalescence kernel described earlier is implemented in the population balance model through a user-defined function. From Figure 4, the Ishii-Zuber and Mills correlations are shown to bound the viscosity of the relevant emulsions. The application of the emulsion viscosity in the interphase momentum exchange term (Equation (3)) is applied through user-defined functions. Three viscosity relationships are evaluated: mixture-averaged viscosity, Ishii-Zuber and Mills. The turbulence is modeled using the Realizable $k-\varepsilon$ mixture turbulence model. The solution methods are phase-coupled SIMPLE for pressure-velocity coupling, second-order upwind discretization for momentum and turbulence, QUICK discretization for the volume fraction equation. The solution is initialized with a zero velocity field and an idealized phase distribution – gas in the freeboard, inlet water fraction in the emulsion phase and clear water layer.

RESULTS

Flow Field

Figure 9 shows the liquid phase pathlines in the separator. The red pathlines are based on the oil phase velocity field, while the blue pathlines are computed from the secondary water phase with the largest diameters. All cases show the typical engineering assumption of a uniform plug flow in the separator is not achieved. The inlet section upstream of the perforated plate shows significant recirculation and mixing. At the lower emulsion viscosities (mixture and Ishii-Zuber) there is good segregation of the pathlines, while at the higher emulsion viscosity (Mills) there is less separation illustrated by increased mixing of the pathlines throughout the settling section. The pathlines curve upwards approaching the weir. The higher viscosity emulsion layer thickness increases along the settling zone upstream of the weir, displacing the oil layer and increasing the water concentration towards the liquid level. Figure 10 plots the vertical profiles of the time-averaged oil-phase axial velocity at the LT9 and LT10 locations shows the velocity field is significantly influenced by the emulsion rheology. The dense emulsion layer causes the oil to accelerate near the free surface.

Oil Distribution

Figure 11 shows the oil distribution in the mid-plane of the separator. The inlet region upstream of the perforated plate shows mixing of the oil-emulsion layer. In the settling zone between the perforated plate and the weir, there is a gradual vertical gradient of water. The mixture-averaged viscosity uses the Schiller-Naumann drag law, which assumes the droplets are settling in a quiescent environment. The interface

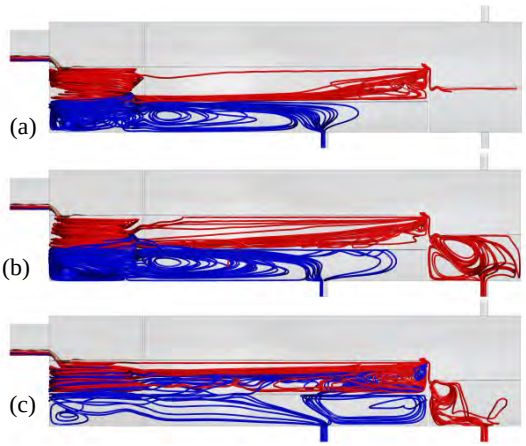

Figure 9. Pathlines of oil (red) and water (blue) on the time-averaged flow field: (a) Mixture-averaged viscosity, (b) Ishii-Zuber viscosity, (c) Mills viscosity.

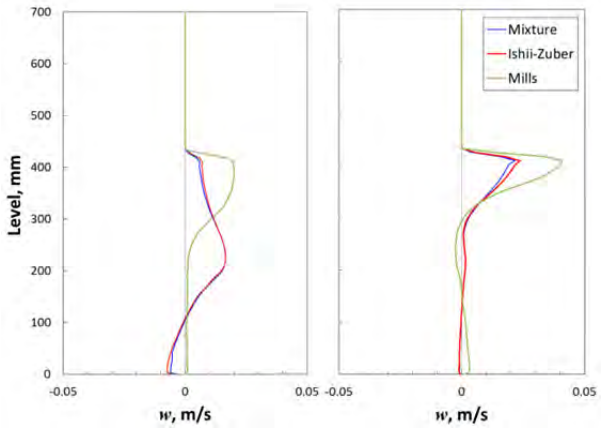

Figure 10. Vertical profiles of the oil axial velocity (time-averaged) at the LT9 and LT10 locations.

layer remains relatively constant throughout the vessel except around the perforated plate. With the higher emulsion viscosity of the Mills relationship (Figure 11(c)), there is a region of low oil and high water concentration above the water layer representative of a dense emulsion layer. The dense emulsion layer increases in thickness toward the end of the settling zone. As the relative viscosity of the emulsion increases, the settling rate slows relative to the coalescence rate allowing water to accumulate. Figure 12 shows the oil distribution in the vessel cross-section at two axial locations corresponding to the LT9 and LT10 level profilers.

Water Fraction

Figure 13 shows the water distribution in the mid-plane of the separator. The water phase gradually separates from the oil with the mixture viscosity and the Ishii-Zuber emulsion viscosity, while the Mills emulsion viscosity shows slow phase separation. Approaching the weir, the water fraction increases near the liquid level. Figure 14 shows the water distribution at the cross-section corresponding to the LT9 and LT10 profiler locations. Plotting the vertical water fraction distribution at the LT10 probe location in Figure 15 shows a distinct water-emulsion interface for each case. With the increased emulsion viscosity with the Mills relationship, a region of higher water fraction is established above the water interface. The water fraction is around 0.53 corresponding to the numerical limit on the relative viscosity of 20.

Relative Viscosity Distribution

Figure 16 shows the relative viscosity distribution in the

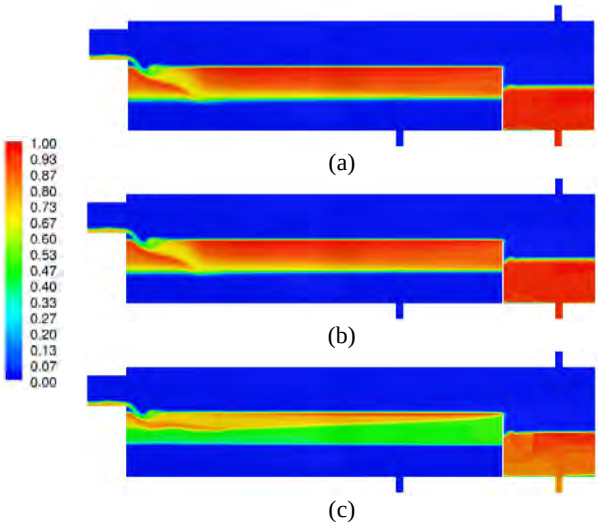

Figure 11. Time-averaged oil fraction distribution: (a) Mixture-averaged viscosity, (b) Ishii-Zuber viscosity, (c) Mills viscosity.

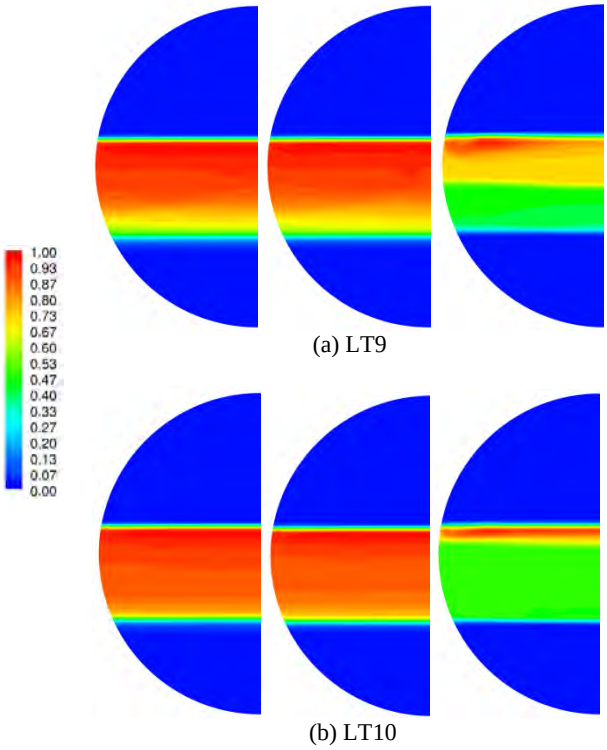

Figure 12. Time-averaged oil fraction distribution at cross-sections LT9 and LT10 (from left to right): Mixture-averaged viscosity, Ishii-Zuber viscosity, and Mills viscosity.

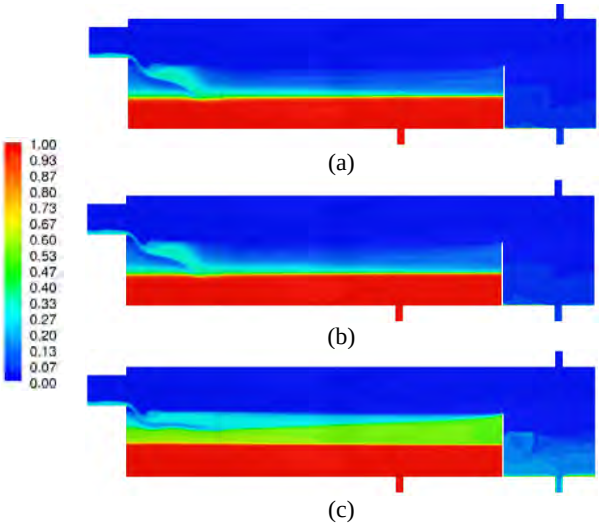

Figure 13. Time-averaged water fraction distribution: (a) Mixture-averaged viscosity, (b) Ishii-Zuber viscosity, (c) Mills viscosity.

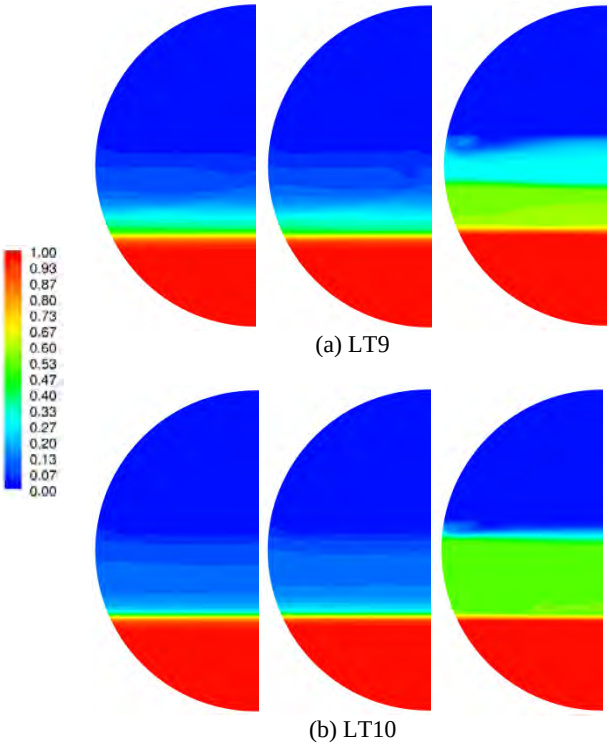

Figure 14. Time-averaged water fraction distribution at cross-sections LT9 and LT10 (from left to right): Mixture-averaged viscosity, Ishii-Zuber viscosity, and Mills viscosity.

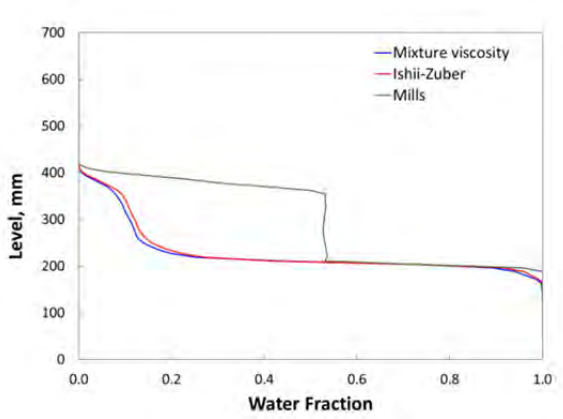

Figure 15. Time-averaged water fraction profiles at LT10 for different emulsion viscosity correlations.

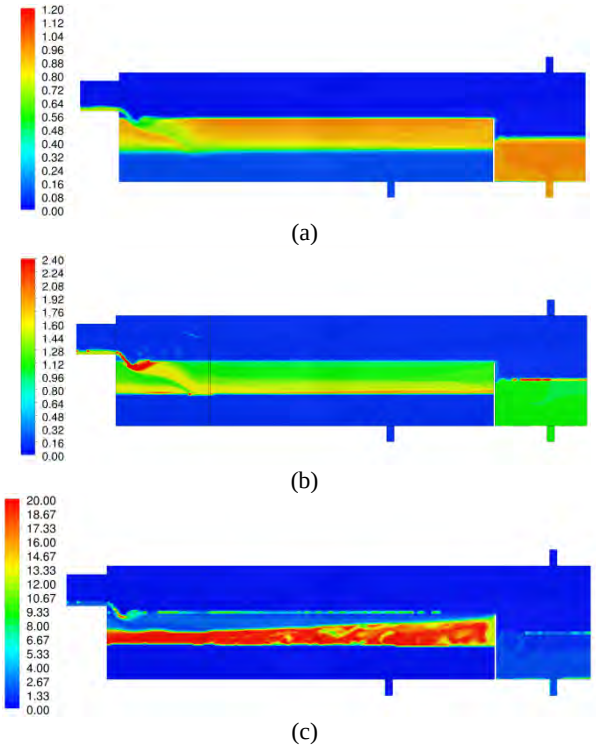

Figure 16. Time-averaged relative viscosity distribution: (a) Mixture-averaged viscosity, (b) Ishii-Zuber viscosity, (c) Mills viscosity.

separator mid-plane. There is an increase in the emulsion viscosity corresponding to the dense emulsion layer above the water interface when an emulsion viscosity relationship is used. The Ishii-Zuber emulsion viscosity is 1.5 times the oil viscosity at the inlet water fraction of 0.27. The Mills emulsion viscosity is 2.2 times at the same water fraction increasing rapidly approaching infinity at the close packing limit of 0.64. The emulsion viscosity relationships show that the hindered settling behavior of the destabilizing emulsion can be reproduced. For this case of an Arab Light crude emulsion with brine (50 g/L) at 45°C, the emulsion viscosity predicted by the Mills relationship is excessive. A rheological characterization is needed to determine the unique viscosity relationship for specific crude oil-water emulsions.

Droplet Diameter Distribution

Figure 17 shows the average water droplet diameter of the three secondary water phases in the vessel cross-section at two axial locations corresponding to the LT9 and LT10 level profilers. As expected, the droplet diameter increases with retention time and water fraction. The larger droplets settle to the interface quickly resulting in a higher droplet diameter above the interface compared with the downstream LT10 location.

Emulsion Layer and Dense-Packed Zone

As the water droplets settle to the water interface in the settling zone, the droplets increase in diameter due to coalescence. The relative viscosity of the emulsion increases slowing separation as the droplets accumulate faster than they coalesce. The region above water interface with higher water concentration is the dense packed zone or DPZ where the water fraction is between the inlet emulsion and unity. Figure 18 compares the water, emulsion and oil layers at the LT9 capacitance profilers to the different CFD predictions with the different emulsion viscosity models. Figure 19 shows the water, emulsion, DPZ and oil layers at the LT10 profiler. While the comparison is qualitative based on how the interface boundaries are determined experimentally, the mixture and Ishii-Zuber reasonably reproduce the DPZ thickness while the Mills relationship over-predicts the DPZ thickness. The emulsion layer thickness is over-estimated by the three emulsion viscosity models suggesting that the water droplets are much larger either from higher coalescence rates or larger droplet sizes entering the separator. Larger droplets will increase the emulsion destabilization rates compared with the model predictions. The water fraction distribution is just one piece of a dataset that must include droplet size and viscosity measurements in order to fully validate the CFD predictions of droplet distribution and emulsion rheology.

Separation Efficiency

The efficiency of water separation from the oil is

$$Separation\ Efficiency, \% = \frac{Q_w|_{Inlet} - Q_w|_{oil\ Outlet}}{Q_w|_{Inlet}} \times 100\%$$

Figure 20 compares the experimentally determined separation efficiency to the different emulsion models. The separation efficiency decreased with the increase in emulsion viscosity showing that the DPZ retards emulsion destabilization. The mixture and Ishii-Zuber emulsion viscosity models under-

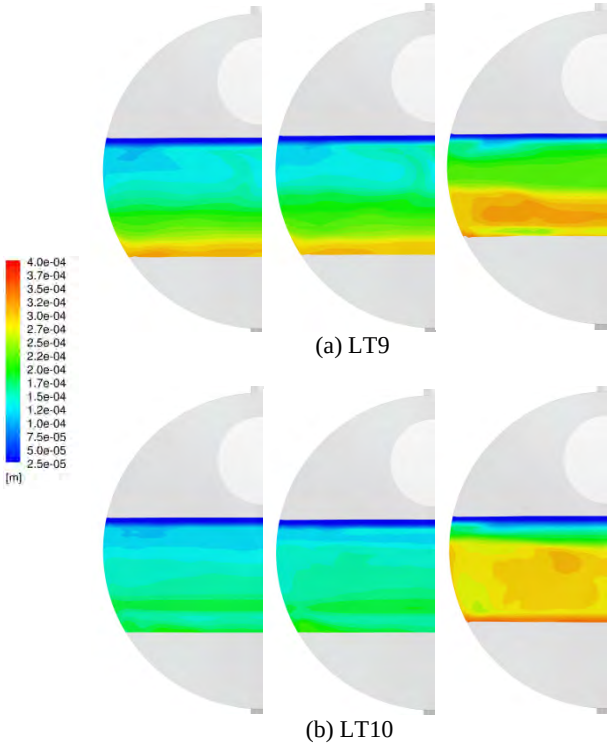

Figure 17. Time-averaged droplet diameter (in m) distribution at cross-sections LT9 and LT10 (from left to right): Mixture-averaged viscosity, Ishii-Zuber viscosity, and Mills viscosity.

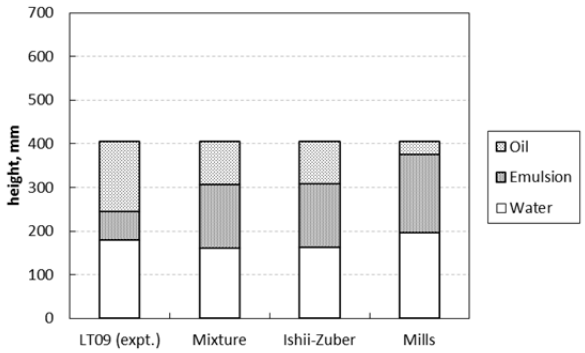

Figure 18. Oil, Emulsion and Water distribution at location LT9.

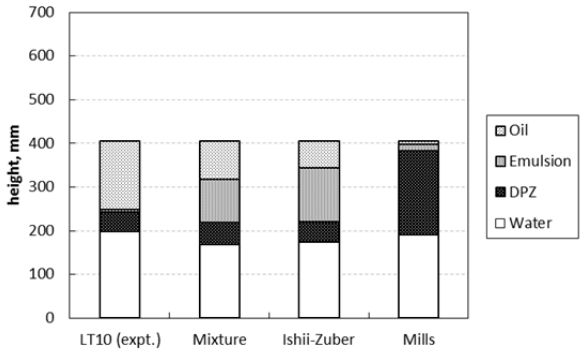

Figure 19. Oil, Emulsion, DPZ and Water distribution at location LT10.

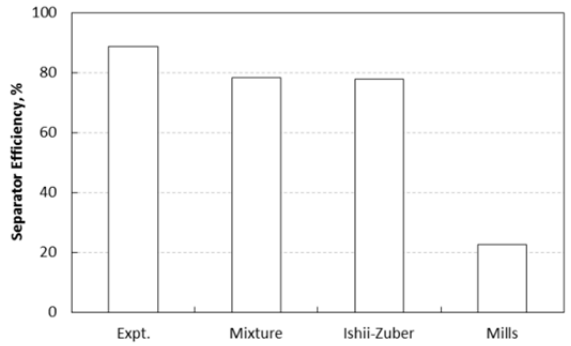

Figure 20. Comparison of experimental and predicted separation efficiency.

predict the separation efficiency. The predicted separation efficiency is influenced the emulsion viscosity relationship, and by other model inputs including the inlet droplet size distribution and the coalescence kernel parameters.

CONCLUSION

In this work, a detailed simulation of a pilot-scale high-pressure three-phase separator has been successfully carried out using the Eulerian multiphase model in ANSYS FLUENT to predict oil-water separation efficiency. The inhomogeneous population balance model was used to describe the evolving droplet size distribution in the polydisperse water phase. Simulations and experiments were performed within the domain of a separator vessel of diameter of 700 *mm* and length of 3000 *mm*. The treatment of the emulsion rheology was implemented through the inter-phase interaction terms between the oil phase and each of the secondary water phases. While there is uncertainty in the experimental water fraction, good agreement of the vertical distributions of the water phase is achieved at different locations in the separator. More detailed experimental data is required to validate the CFD models. The inlet multiphase flow must be adequately characterized for phase and droplet size distribution. Droplet coalescence and breakage should be incorporated and be specifically defined for the horizontal multiphase separator configuration. The CFD methodology presented here is a step toward predicting the dense emulsion layer thickness above the water interface, the evolution of the droplets size distribution through the separator, and the oil-water separation efficiency. More study is needed to include a more accurate description of the emulsion rheology and the coalescence and breakage mechanisms, while taking in to consideration the complexity of crude oil inhomogeneity, pH, salinity, asphaltene content or impurities in the water, and the surface-active compounds added to the produced fluids.

ACKNOWLEDGEMENTS

The authors acknowledge the Saudi Arabian Oil Company (Saudi Aramco) for supporting and granting permission to present and publish this article. The authors also acknowledge IFPEN for conducting the experiments and to TOTAL for their role in coordinating the experimental program. The authors would also like to acknowledge ANSYS for their support on the PID controller user-defined function and Scheme file.

REFERENCES

ANSYS Inc. *ANSYS FLUENT™ Theory Guide.* Canonsburg, PA: ANSYS Inc, 2012.

BRINKMAN, H.C. "The viscosity of concentrated suspensions and solutions." *J. Chem. Phys.* 20 (1952): 571.

FRANK, T., P.J. ZWART, J-M. SHI, E. KREPPER, D. LUCAS, and U. ROHDE. "Inhomogeneous MUSIG Model - a Population Balance Approach for Polydispersed Bubbly Flows." *International Conference on Nuclear Energy for New Europe, September 5-8.* Bled, Slovenia, 2005.

FRISING, T., NOIK, C., and DALMAZZONE, C. "The Liquid/Liquid Sedimentation Process; From Droplet Coalescence to Technologically Enhanced Water/Oil Emulsion Gravity Separators: A Review." *Journal of Dispersion Science and Technology* 27 (2006). 1035-1057.

GARCIA, F., J.M. GARCIA, R. GARCIA, and D.D. JOSEPH. "Friction factor improved correlations for laminar and turbulent gas-liquid flow in horizontal pipelines." *International Journal of Multiphase Flow* 33 (2007): 1320-1336.

GRIMES, B.A. "Population Balance Model for Batch Gravity Separation of Crude Oil and Water Emulsions. Part I: Model Formulation." *Journal of Dispersion Science and Technology* 33 (2012): 578-590.

HALLANGER, A., F. SOENSTABOE, and T. KNUTSEN. "A Simulation Model for Three-Phase Gravity Separators (SPE 36644)." *SPE Annual Technical Conference and Exhibition, 6-9 October 1996.* Denver, Colorado, USA: Society of Petroleum Engineers, 1996. 695-706.

HANSEN, E.W.M., and G.J. RØRTVEIT. "Numerical Simulation of Fluid Mechanisms and Separation Behavior in Offshore Gravity Separators." Chap. 16 in *Emulsions and Emulsion Stability*, edited by J. Sjöblom, 593-605. CRC Press, 2005.

HANSEN, E.W.M., et al. "Fluid Flow Modeling of Gravity Separators." *5th International Conference on Multi-Phase Production.* Cannes, 1991.

HENSCKE, M., L.H. SCHLIEPER, and A. PFENNIG. "Determination of a Coalescence Parameter from batch-

Settling Experiments." *Chemical Engineering Science* 85 (2002): 369-378.

HINZE, J.O. "Fundamentals of the hydrodynamic mechanism of splitting in dispersion processes." *AIChE J.* 1, no. 3 (1955): 289-295.

ISHII, M., and N. ZUBER. "Drag Coefficient and Relative Velocity in Bubbly, Droplet or Particulate Flows." *AIChE J.* 25 (1979): 843-855.

KESKIN, C., H.-Q. ZHANG, and C. SARICA. "Identification and Classification of New Three-Phase Gas/Oil/Water Flow Patterns." *SPE Annual Technical Conference and Exhibition, 11-14 November*. Anaheim, California, U.S.A.: Society of Petroleum Engineers, 2007.

KHAROUA, N., L. KHEZZAR, and H. SAADAWI. "Application of CFD to Debottleneck Production Separators in a Major Oil Field in the Middle East (SPE 158201)." *SPE Annual Technical Conference and Exhibition, 8-10 October*. San Antonio, Texas, USA: Society of Petroleum Engineers, 2012.

KOKAL, S. "Crude-Oil Emulsions: A State of the Art Review." *SPE Production & Facilities* (Society of Petroluem Engineers) 20, no. 1 (2005): 5-13.

KRALOVA, I., SJÖBLOM, G. ØYE, S. SIMON, B. GRIMES, AND K. PASO. "Heavy Crude Oils/Particle Stabilized Emulsions." *Advances in Colloid and Interface Science* 169 (2011): 106-127.

KRIEGER, I.M., and I.M. DOUGHERTY. "A mechanism for non-Newtonian flow in suspensions of rigid spheres." *Trans. Soc. Rheol.* 3 (1959): 137.

LALEH, A.P., W.Y. SVRCEK, and W.D. MONNERY. "Design and CFD Studies of Multiphase Separators - A Review." *The Canadian Journal of Chemical Engineering* 90 (2012): 1547-1560.

LIAO, Y., and D. LUCAS. "A literature review on mechanisms and models for the coalescence process of fluid particles." *Chemical Engineering Science* 65 (2010): 2851-2864.

LUO, H., and H.F. SVENDSEN. "Theoretical Model for Drop and Bubble Breakage in Turbulent Dispersions." *AIChE J.* 42, no. 5 (1996): 1225-1233.

MARSDEN, S., and M. MAD. "Stability Of Concentrated Crude Oil-In-Water Emulsions As A Function Of Shear Rate, Temperature And Oil Concentration." *26th Annual Technical Meeting of the Petroleum Society of CIM, June 11-13*. Banff, Alberta, Canada: PETROLEUM SOCIETY OF CIM, 1975.

MILLS, P. "Non-Newtonian behaviour of flocculated suspensions." *J. Physique Lett.* 46 (1985): 301-309.

PAGNIER, P., C. NOIK, P. MAUREL, A. RICORDEAU, and J.-L. A. VOLLE. "Multiphase Loop Tests for Subsea Separation-Unit Development." *Paper SPE 115963 presented at SPE Annual Technical Conference and Exhibition.* Denver, Colorado, USA, 21-24 September: Society of Petroleum Engineers, 2008.

RAMKRISHNA, D. *Population Balances: theory and Applications to Particulate Systems in Engineering.* eBook: Academic Press, 2000.

SANFELD, A., and A. STEINCHEN. "Emulsion stability, from dilute to dense emulsions - Role of drops deformation." *Advances in Colloid and Interface Science* 140 (2008): 1-65.

SANYAL, J., S. OZARKAR, and F. LIU. "A Comprehensive CFD Strategy for the Simulation of Dense, Polydisperse Granular Flow in Fluidized Bed Reactors." *8th International Conference on Multiphase Flow (ICMF 2013), May 26 - 31*. Jeju, Korea, 2013.

SCHULLER, R.B., T. GUNDERSEN, M. HALLERAKER, and B. ENGEBRETSEN. "Measurement of water concentration in oil/water dispersions with a circular single-electrode capacitance probe." *Instrumentation and Measurement, IEEE Transactions* 53, no. 5 (2004): 1378-1383.

SIMONS, S., M.M.R. WILLIAMS, and J.S. CASSELL. "A kernel for combined Brownian and gravitational coagulation." *Journal of Aerosol Science* 17, no. 5 (1986): 789-793.

VIELMA, M., S. ATMACA, C. SARICA, and H. ZHANG. "Characterization of Oil/Water flows in horizontal pipes." *SPE Projects, Facilities & construction*, 2008: 1 - 21.

VILAGINES, R.D., and A.R. AKHRAS. "Three-phase Flows Simulation for Improving Design of Gravity Separation Vessels (134090)." *SPE Annual Technical Conference and Exhibition, 19-22 September 2010.* Florence, Italy: Society of Petroleum Engineers, 2010.